6-2012

Exploiting tree shadows on snow for estimating forest basal area using Landsat data

P. T. Wolter
Iowa State University, ptwolter@iastate.edu

E. A. Berkley
United States Fish and Wildlife Service

S. D. Peckham
University of Wisconsin - Madison

A. Singh
University of Wisconsin-Madison

P. A. Townsend
University of Wisconsin-Madison

Exploiting tree shadows on snow for estimating forest basal area using Landsat data

Abstract
Basal area (BA) is a basic structural and ecological attribute of forests that is often used to describe forest composition, estimate volume of wood, and guide management decisions. BA is the sum of cross-sectional area of trees measured at 1.37 m above ground surface, per unit area, and is most commonly measured *in-situ*. The objective of this study was to supply estimates of BA for oak woodlands and savannas on the 12,828.5 ha Sherburne National Wildlife Refuge in Central Minnesota to guide management efforts. We used winter and summer Landsat imagery, combined with field measurements, to assess the potential for improving forest BA estimates by taking advantage of the high spectral contrast between sunlit snow, forest canopy elements, and shadows projected onto snow ground cover. We explained up to 90% of measured variation in BA using partial least squares regression models calibrated using single- and multiple-date winter Landsat data ($R^2 = 0.898$, RMSE = 2.79 m^2ha^{-1}), which performed better than models calibrated using summer imagery ($R^2 = 0.762$, RMSE = 3.85 m^2ha^{-1}). Success of the winter-based BA models may be driven, in part, by potential geometric/allometric relationships between cast shadow and forest BA, but definitive proof of this is a topic for future research. This method of BA estimation is not refuge-specific and may be extended for regional use to manage oak forest wherever winter snow coverage is consistent. Additional research is needed to determine the degree of robustness to variations in the empirical relationship between BA and tree shading patterns across different forest functional types.

Keywords
Forest basal area, Landsat, Multi-temporal, Winter, Snow cover, Tree shadows, Shadow area difference, Sun elevation angle, Partial least squares regression, Oak savanna

Disciplines
Forest Management | Natural Resources and Conservation | Natural Resources Management and Policy | Other Environmental Sciences

Comments
This article is from *Remote Sensing of Environment* 121 (2012): 69, doi: 10.1016/j.rse.2012.01.008.

Remote Sensing of Environment 121 (2012) 69–79

Contents lists available at SciVerse ScienceDirect

Remote Sensing of Environment

journal homepage: www.elsevier.com/locate/rse

Exploiting tree shadows on snow for estimating forest basal area using Landsat data

P.T. Wolter [a,c,*], E.A. Berkley [b], S.D. Peckham [c], A. Singh [c], P.A. Townsend [c]

[a] Department of Natural Resource Ecology and Management, Iowa State University, 339 Science II, Ames, IA 50011, United States
[b] United States Fish and Wildlife Service, Sherburne National Wildlife Refuge, 17076 293 Ave., Zimmerman, MN 55398, United States
[c] Department of Forest and Wildlife Ecology, University of Wisconsin-Madison, 1630 Linden Drive (Suite 224), Madison, WI 53706, United States

ARTICLE INFO

Article history:
Received 17 June 2011
Received in revised form 20 December 2011
Accepted 7 January 2012
Available online 17 February 2012

Keywords:
Forest basal area
Landsat
Multi-temporal
Winter
Snow cover
Tree shadows
Shadow area difference
Sun elevation angle
Partial least squares regression
Oak savanna

ABSTRACT

Basal area (BA) is a basic structural and ecological attribute of forests that is often used to describe forest composition, estimate volume of wood, and guide management decisions. BA is the sum of cross-sectional area of trees measured at 1.37 m above ground surface, per unit area, and is most commonly measured *in-situ*. The objective of this study was to supply estimates of BA for oak woodlands and savannas on the 12,828.5 ha Sherburne National Wildlife Refuge in Central Minnesota to guide management efforts. We used winter and summer Landsat imagery, combined with field measurements, to assess the potential for improving forest BA estimates by taking advantage of the high spectral contrast between sunlit snow, forest canopy elements, and shadows projected onto snow ground cover. We explained up to 90% of measured variation in BA using partial least squares regression models calibrated using single- and multiple-date winter Landsat data ($R^2 = 0.898$, RMSE = 2.79 m^2ha^{-1}), which performed better than models calibrated using summer imagery ($R^2 = 0.762$, RMSE = 3.85 m^2ha^{-1}). Success of the winter-based BA models may be driven, in part, by potential geometric/allometric relationships between cast shadow and forest BA, but definitive proof of this is a topic for future research. This method of BA estimation is not refuge-specific and may be extended for regional use to manage oak forest wherever winter snow coverage is consistent. Additional research is needed to determine the degree of robustness to variations in the empirical relationship between BA and tree shading patterns across different forest functional types.

1. Introduction

Basal area (BA) is a forest structural attribute that is included in most ground-based forest inventories. It consists of the sum of tree trunk cross-sectional area measured 1.37 m above ground for a given area. BA is used in forest management to describe presence of trees, to estimate tree volume, and to inform management decisions (Ginrich, 1967). Forest BA is also an important ecological attribute used to estimate forest productivity (Burrows et al., 2003), understand ecosystem structure and function (Marshall & Waring, 1986; Pacala & Deutschman, 1995; Whittaker et al., 1974), as a surrogate for tracking forest carbon (Brown et al., 1989; Phillips et al., 1998), and as a metric to understand the ecology and habitat requirements of forest fauna (e.g., Blais, 1958; Niemi & Hanowski, 1984; Pastor et al., 1998; Sharov et al., 1999). As a result, much effort is devoted to estimating and mapping forest BA using satellite remote sensing data (Brockhaus et al., 1992; Hudak et al., 2006; Hyyppä et al., 2000; McRoberts, 2008; McRoberts et al., 2007; Wolter & Townsend, 2011; Wolter et al., 2008, 2009; Wulder et al., 2000).

Optical remote sensing-based models used to estimate forest BA in northern latitudes have typically explained less than 75% of the variability in ground calibration data (Cohen & Spies, 1992; Franco-Lopez et al., 2001; Franklin, 1986; Hyyppä et al., 2000; Moisen et al., 2006; Wolter & Townsend, 2011; Wolter et al., 2008, 2009). And, while lidar estimates of forest biophysical parameters including BA are increasingly precise (Anderson et al., 2008; Lim et al., 2003), region-wide application of lidar is limited due to high cost per area covered (Zheng et al., 2008). In this paper, we highlight an approach to remote sensing-based mapping of deciduous forest BA in central Minnesota using multi-temporal winter Landsat imagery (with snow cover) and then compare these results to those obtained using leaf-on, summer Landsat imagery.

2. Background

Since Ptolemy (AD 90–168) people have used shadow length to calculate height of objects and to estimate latitude (see van Brummelen & Butler, 1997). On sunny days, a tree's height (H) can be estimated by simultaneously measuring sun elevation angle (θ) and the tree shadow length (L) using the formula $L \cdot \tan(\theta) = H$. In sparse forests (e.g., oak woodlands), under low sun elevation, tree shadows can cover large fractions of the ground (Vikhamar et al., 2004). Because tree shadows are a combination of shaded tree and

* Corresponding author at: Department of Natural Resource Ecology and Management, Iowa State University, 339 Science II, Ames, IA 50011, United States.
E-mail address: ptwolter@iastate.edu (P.T. Wolter).

0034-4257/$ – see front matter © 2012 Elsevier Inc. All rights reserved.
doi:10.1016/j.rse.2012.01.008

ground, attributes of single tree shadows (length or area, Fig. 1A) should correlate with tree crown diameter, crown height, and stem diameter to a degree that may facilitate estimation and mapping of forest biomass (Oladi, 2001). In the 1940s, the U.S. Forest Service took advantage of such relationships between tree shadow length, tree height, and tree volume (known as the tree-shadow technique) to systematically develop estimates of wood volume for large tracts of forest in the northeastern U.S. using aerial photo reconnaissance imagery (Seeley, 1942; Rogers, 1949).

With the arrival of satellite sensors such as Landsat, new modeling tools were developed to understand vegetation reflectance behavior and pave the way for repeatable, systematic quantification of biophysical characteristics of forest vegetation for large areas, such as crown size, tree density, canopy cover, and biomass (e.g., Badhwar et al., 1985; Suits, 1972; Verhoef, 1984). One family of canopy reflectance models, referred to as "geometric–optical" (G–O, Li & Strahler, 1985, 1992), treats vegetation cover as a set of discrete objects on a planar surface, where each object (sunlit and shaded tree crowns and forest floor) must possess a distinct spectral signature to yield accurate estimates of forest structure. Reflectance is modeled as a function of tree position and pattern, solar illumination angle, shadows, and ground visible through simulated canopies from a given observation point; where "shadow is a key component in the model to provide three-dimensional structure information" (Wu and Strahler, 1994). With careful field calibration and correction, the G–O model can be inverted to provide direct estimates of crown size and spacing parameters from remote sensing images; even when pixel resolution is larger than individual tree crown sizes (Franklin and Strahler, 1988; Strahler et al., 1988). As a practical test of G–O model inversion technique, Wu and Strahler (1994) evaluated summer and winter Landsat Thematic Mapper (TM) imagery. The latter was considered ideal for this test as winter conditions (with snow) closely approximated key requirements of their G–O model: strong and distinct spectral contrast between sunlit and shaded forest canopy and forest floor components. They found that models calibrated using winter TM imagery performed well, and that better results would have been possible if the model explicitly handled canopy self-shading, which is greater in winter with lower sun elevation angles compared to other months. Later versions of G–O models were improved by specifically incorporating tree self-shading (e.g., Li and Strahler, 1992).

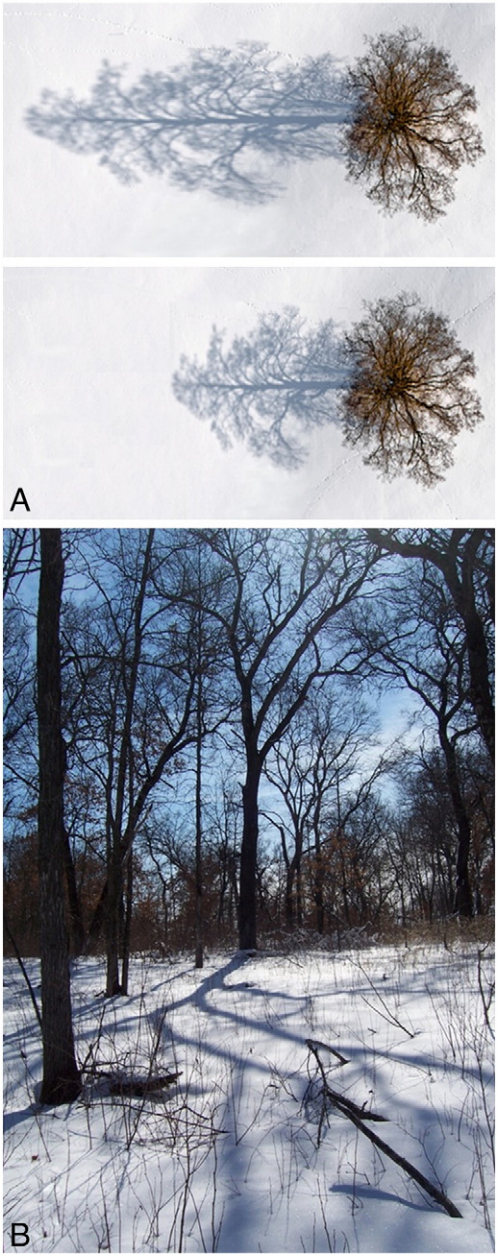

Fig. 1. Nadir views of tree shadow length and area differences (A) cast onto snow cover at low (top) and high (bottom) sun elevation angle during winter months. Oak savanna at Sherburne NWR in central Minnesota showing tree shadows (B) on snow (taken 3/19/2011 at 15:45 UTC).

Because tree height is allometrically related to other structural parameters, such as bole diameter at breast height (DBH) and biomass (Jenkins et al., 2003; Perala & Alban, 1994), high spatial resolution image data have been used to derive estimates of tree crown area, crown diameter, and DBH with moderate accuracy by focusing specifically on canopy shadow characteristics (Greenberg et al., 2005; Song, 2007; Song & Woodcock, 2003). Medium resolution (5 and 10 m) optical satellite sensor data have also been used to leverage tree shadow characteristics to assist estimation of forest structural characteristics, including BA (Wolter et al., 2009).

In multi-temporal studies, winter Landsat imagery (with snow ground cover) produced stronger predictors of forest BA than other seasons analyzed (Franco-Lopez et al., 2001; Wolter et al., 2008). This results from snow beneath a forest canopy concealing spectrally variable undergrowth and litter that can confound overstory structural signatures (e.g., Brown et al., 2000; Chen & Cihlar, 1996; White et al., 1995). As noted earlier, snow provides a uniformly bright background that accentuates tree crowns and their shadows (Seely, 1949; Sayn-Wittgenstein, 1961) and associated spectral factors linked to forest density (Wu and Strahler, 1994), height (Wolter et al., 2009), and age (Horler & Ahern, 1986).

High spatial resolution sensor data (e.g., $\leq$4 m pixels) can be used to derive forest structural attributes through analysis of tree-wise shadow characteristics (Greenberg et al., 2005; Leboeuf et al., 2007; Peddle et al., 1999). However, as the need to repeatedly quantify forest structural attributes for large areas arises, financial and computational costs associated with high spatial resolution sensor data may preclude their use in regional-scale research and resource management efforts. In this paper we demonstrate a unique approach to estimating deciduous forest BA by leveraging 1) relationships between tree shadows and forest structural parameters (Greenberg et al., 2005; Ozdemir, 2008; Wu and Strahler, 1994) and 2) the "strong and distinct spectral contrast" deemed necessary for accurate, remote sensing-based, parameter estimation that winter imagery (with snow ground cover) provides (Wu and Strahler, 1994). Our hypothesis hinges on the observation that while the spectral properties of forest constituents (sunlit and shaded snow, tree trunks, and branches) during winter are different (Vikhamar & Solberg, 2002), the radiance or reflectance of these forest targets does not change substantially from one winter month to the next (Vikhamar & Solberg, 2002).

The illumination fraction of vertical-tending components of the above ground biomass (AGB) visible to nadir-looking sensors changes

with solar elevation angle, but we postulate that associated change in both horizontal ground-shadow and sun-lit snow area produced by the AGB (tree trunks and branches) has a greater effect on overall, integrated forest reflectance detected by Landsat (e.g., Fig. 1). Spatially integrated forest reflectance received by an optical, satellite sensor during winter months is a complex mix of sun-lit/shaded tree canopies and forest floor; compounded by varying degrees of tree-to-tree self-shading (Wu and Strahler, 1994). However, if we accept the assumption above, then for northern latitudes where continuous snow ground cover through the winter is the norm, difference indices derived using two or more Landsat images (dynamic) having substantially different solar elevation ephemeris should be biased toward enhancement of differences in illumination of the forest floor. Because differences in forest floor shadow or illumination are, in part, related to sun elevation angle, tree size, and stem density, it may be possible through multi-temporal image analysis to augment empirical spectral relationships with forest BA over that possible using single-date (static) image analyses.

In this study, we extend the use of iterative exclusion partial least squares (xPLS) regression to evaluate 66 winter and 38 summer Landsat predictor variables to answer two main questions. First, will forest BA models developed using two and three winter Landsat images (with snow ground cover and differing solar elevation) outperform separate analysis of single winter images for estimating BA? Second, are BA models derived using winter Landsat data (single date or multi-temporal) superior to BA models developed using summer Landsat data?

3. Methods

3.1. Study area

Sherburne National Wildlife Refuge (SNWR) is located on the gently rolling to flat Anoka Sandplain in Central Minnesota (Fig. 2, N 45.49° Lat., W 93.73° Lon.). Oak savanna habitat at SNWR, like oak savanna elsewhere, is a fire-dependent, dynamic community characterized by scattered trees or groves of trees, mostly comprised of oak species with canopy cover ranging from 5 to 96% and basal area (BA) 2–34 m^2 ha^{-1}, but more typically canopy cover is between 25 and 50% (Fig. 1B), with BA ~12 m^2 ha^{-1}. Estimated average height of the mature forest overstory is ~16.76 m (55 ft.). Canopy cover can vary at small-scales (stand level) where areas of both scattered trees and areas with groves of trees are present within a single stand. Bur oak (*Q. macrocarpa*) is typically the dominant tree species interspersed with red oak (*Q. rubra*) or northern pin oak (*Q. elipsoidalis*) (Buchanan, 1996; Law et al., 1994), which readily hybridize in this area (Swain, 1972; Tester, 1989). The understory vegetation is sparse or patchy with both native grasses (25–100%) and forbs (5–50%) (MNDNR, 2005). Northern pin oak is sometimes present as a secondary tree species in the overstory or in the shrub layer. The shrub layer is typically dominated by American hazelnut (*Corylus americana*) or oak sprouts (*Quercus* sp.) and is patchy to continuous (30–100%). The ground layer is composed mostly of native forbs and woody plants characteristic of oak forests, but also some prairie and savanna forbs and graminoids as well (Wovcha et al., 1995). The extent of "prairie" openings is less than 30%.

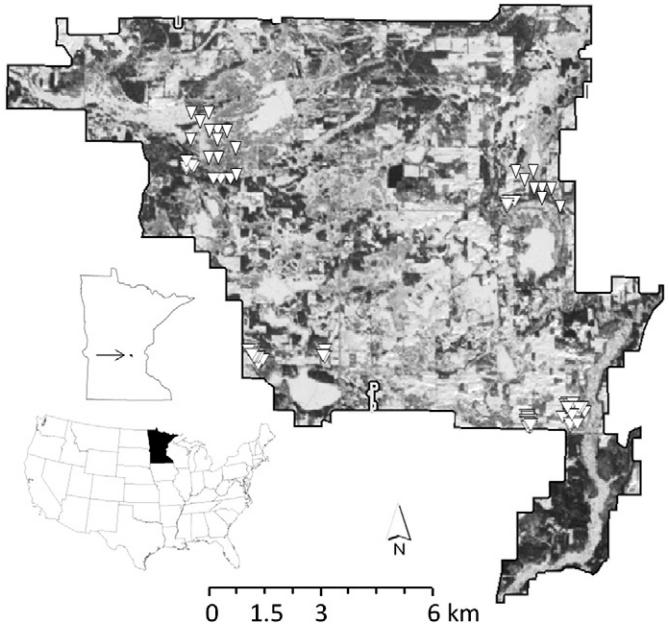

Fig. 2. Landsat-5 image (3/10/2008, band 2) of Sherburne NWR in central Minnesota showing field plot locations (triangles). The refuge covers an area of 124 km^2 (30,700 ac) and consists of oak woodlands, savannas, and prairies.

3.2. Field data

Forested areas were sampled in 2009 (60 plots) by the authors and other SNWR personnel. Field plot data consisted of a total five variable radius (Grosenbaugh, 1952) subplots: one located at the intersection and one at each of the four end points of two crossing 60 m transect lines placed near center of large (≥4.4 ha), homogenous stands (Fig. 2). Plot locations were determined randomly within three BA ranges: 21 low BA plots (range 2.4–15.6 m^2 ha^{-1}), 16 medium BA plots (range 16–23 m^2 ha^{-1}), and 23 high BA plots (range 24–34.4 m^2 ha^{-1}). Sufficient stand size and homogeneity assured that stand edge effects were minimized during analysis, and that image misregistration errors were inconsequential. We recorded the location (UTM zone 15) of each plot's center to within 3 m (2dRMS) using a WAAS enabled Garmin eTrex (Garmin International, Inc., Olathe, KS, U.S.A.). Total BA (all live and dead trees) was measured at each subplot using a metric basal area factor (BAF) 2 prism. Total BA data were then used as the dependent variable to develop partial least squares (PLS) regression models to estimate forest BA using Landsat sensor data.

3.3. Landsat data

Five Landsat Thematic Mapper (TM) images (three winter and two summers images) were acquired for this study based on temporal proximity to field data collection (summer 2009). Henceforth, the five Landsat images will be referred using letter codes: January (J), February (F), March (M), June (U), and August (A) (Table 1). All five Landsat images were downloaded from the USGS Earth Resources Observation and Science Center (EROS) web site (source: http://glovis.usgs.gov/) in UTM zone 15 coordinates. These 30 m Landsat images are convenient as they are precision-orthorectified and geo-corrected using Global Land Cover Facility (GLCF) GeoCover data (source: www.landcover.org). The five Landsat images used in this study exhibited excellent pixel co-registration with each other. Each image was converted to top of atmosphere reflectance using published sensor calibration coefficients (Thome et al., 2004). Because topography is known to influence Earth surface reflectance (Culvenor & Coops, 1999; Dozier, 1989; Olyphant, 1984), all images were topographically adjusted with a lambertian correction methodology (see Riaño et al., 2003) using a 30 m digital elevation model (DEM, source: http://ned.usgs.gov/) and scene-specific sun position information (Table 1). Because only relative differences in tree-to-ground shadow proportion were of interest, scene-to-scene radiometric normalizations were not performed.

Weather conditions (source: http://climate.umn.edu/) at SNWR during the time of Landsat sensor overpass were noted for later interpretation, including peak wind speeds between the most recent snowfall event prior to the date of image acquisition (Table 1).

Table 1
Dates and corresponding letter codes for the five Landsat TM images acquired for the Sherburne NWR. Solar ephemeris, snow depth, maximum wind since last snowfall, and temperature at the time of sensor overpass are shown.

Image date	Image code	Solar elevation	Solar azimuth	Snow depth (cm)	Last snowfall	Wind speed (km/h)	Temp. (°C)
1/8/2009	J	18.50	156.80	42.5	1/4/2009	59.0	−18.9
2/23/2008	F	30.04	152.27	27.5	2/14/2008	44.0	−12.2
3/10/2008	M	36.05	150.64	17.5	3/5/2008	48.0	−7.2
6/30/2008	U	60.70	133.83	–	–	–	23.9
8/17/2008	A	51.82	142.06	–	–	–	26.7

In addition to each image's six reflective bands (TM1–TM5 and TM7) and commonly used indices (normalized difference vegetation index, NDVI, Rouse et al., 1974; soil adjusted vegetation index, SAVI, Huete, 1988; and simple ratio, SR, Jordan, 1969), shortwave infrared-based (SWIR; TM5 and TM7) indices (moisture stress index, MSI, Rock et al., 1986; normalized burn ratio, NBR, Lopez-Garcia and Caselles, 1991; Key & Benson, 2005; reflectance absorption index, RA, Arzani & King, 1997; and shortwave infrared visible ratio, SVR, Wolter et al., 2008) were included in these analyses (Table 2) because formulations using SWIR are known to be sensitive to forest BA (Horler & Ahern, 1986; Olsson, 1994; Wolter et al., 2008). In addition, near-infrared (NIR) and SWIR regions of the electromagnetic spectrum experience negligible water vapor and Rayleigh scattering effects (attenuation) compared to visible wavelengths (Larsen & Stamnes, 2005; Liang et al., 2002), and therefore exhibit less interference for identifying contrast between shaded and sunlit snow under clear sky conditions. Disproportionate diffuse irradiance or 'skylight' (Dubayah, 1994) in the visible wavelengths accounts for partial illumination of geometric or hard shadows, potentially lowering contrast sensitivity between shaded and fully illuminated forest floor. For this reason, indices composed of NIR, SWIR, or contrasts between these wavelengths and visible wavelengths may enhance detectability of forest floor shadow fraction and improve the detection of empirical relationships with forest BA. While normalized difference ratios ND25, also known as the normalized difference snow index (NDSI, Dozier, 1989), and ND42 cover these coarse spectral differences, ND21, ND31, ND32, and AI (Wolter and Townsend, 2011) were tested in a speculative fashion to identify visible band indices (Table 2) that may exhibit wavelength-specific variation in snow reflectance saturation (see Dozier, 1989) that varies with forest BA.

It should be noted that while portions of the NIR region (1.0–1.3 μm) of the electromagnetic spectrum are known to be especially responsive to snow grain-size, Landsat-5's NIR band (TM4, 0.76–0.90 μm) is only modestly sensitive to this parameter (Painter et al., 2003). SWIR sensitivity to snow grain size is most apparent at warmer temperatures (closer to freezing), which produce larger (e.g., ≥250 μm) surface snow grains than lower sub-freezing temperatures (Jordan, 1991; Painter et al., 2003). Both NIR and SWIR wavelengths are sensitive to the development of liquid water film around surface grains of a snow pack once the temperature exceeds freezing (Gupta et al., 2005). In our study, temperature effects on snow should be minimal since recorded maximum daytime temperatures were all well below 0.0 °C prior to the winter image acquisition dates. The effect of illumination geometry on snow reflectance can be substantial in the NIR and SWIR for smaller (~50 μm) snow grain sizes (Dozier, 1989), but we have assumed in this study that spectral sensitivity to snow grain size was minimal compared to shadow/illumination fraction and above ground biomass signatures.

Winter, cross-date band ratios (RAT prefix in tables and figures) and differences (DIFF prefix), as well as SVR differences, are heuristic formulations to capture forest reflectance changes specifically associated with variation in sun elevation angle (Tables 1, 2). For the DIFF and RAT formulations, TM2, TM4 and TM5 were chosen for best contrast between shaded vs. sunlit snow (see Dozier, 1989; Rosenthal and Dozier, 1996; Vikhamar et al., 2004). For overall consistency, temporal differences and ratios between summer image dates were also computed and analyzed (Table 2). The associated suffix (JF, JM, FM, or UA) refers to the dates of imagery used in the temporal difference and ratio formulations. For example, DIFF2_JF is the difference between TM2_J and TM2_F or, specifically, the difference in green reflectance between January and February, respectively (Tables 1, 2).

In all, there are 63 and 36 Landsat predictor variables from the three winter images and two summer images, respectively. The USGS 30 m DEM was used to produce five shaded relief images (three winters and two summers) based on solar ephemeris information corresponding to the respective Landsat overpass times and dates. Although image topographic corrections were applied to adjust for reduced reflectance of the incident solar irradiance due to local terrain, such corrections do not adjust for full geometric shadows (often referred to as hard shadow) or potential differences in contrast between sun-lit and hard-shaded surfaces. Hence, date-specific, shaded relief layers were added as explanatory variables to account for local slope- and azimuth-related effects on tree shadow length (see Vikhamar et al., 2004). All winter Landsat image combinations (J, F,

Table 2
Winter and summer Landsat image variables used to estimate forest basal area (BA). Separate image bands (TM1–TM5 and TM7) for each date were also used as predictor variables, but are not specifically listed below. Suffix letter codes J, F, M, U, and A represent January, February, March, June, and August, respectively (see Table 1 for specific dates).

Winter		Summer	
Indices	Formulation	Indices	Formulation
NDVI	(TM4 − TM3)/(TM4 + TM3)	AI	TM3/TM1
ND42	(TM4 − TM2)/(TM4 + TM2)	MSI	TM5/TM4
ND32	(TM3 − TM2)/(TM3 + TM2)	NDVI	(TM4 − TM3)/(TM4 + TM3)
ND25	(TM2 − TM5)/(TM2 + TM5)	NBR	(TM4 − TM7)/(TM4 + TM7)
ND31	(TM3 − TM1)/(TM3 + TM1)	RA	TM4/(TM3 + TM5)
ND21	(TM2 − TM1)/(TM2 + TM1)	SAVI	(1.5 * (TM4 − TM3))/(TM4 + TM3 + 0.5)
SVR	(TM5 + TM7)/(TM1 + TM2 + TM3) * 1.5	SR	TM4/TM3
MSI	TM5/TM4	SVR	(TM5 + TM7)/(TM1 + TM2 + TM3) * 1.5
SVR_JF	SVR_F − SVR_J	SVR7	(TM7)/(TM1 + TM2 + TM3) * 3
SVR_JM	SVR_M − SVR_J	DIFF2_UA	TM2_A − TM2_U
SVR_FM	SVR_M − SVR_F	DIFF4_UA	TM4_A − TM4_U
DIFF5_JF	TM5_F − TM5_J	DIFF5_UA	TM5_A − TM5_U
DIFF5_JM	TM5_M − TM5_J	RAT2_UA	TM2_A/TM2_U
DIFF5_FM	TM5_M − TM5_F	RAT4_UA	TM4_A/TM4_U
RAT5_JF	TM5_F/TM5_J	RAT5_UA	TM5_A/TM5_U
RAT5_JM	TM5_M/TM5_J		
RAT5_FM	TM5_M/TM5_F		
DIFF4_JF	TM4_F − TM4_J		
DIFF4_JM	TM4_M − TM4_J		
DIFF4_FM	TM4_M − TM4_F		
RAT4_JF	TM4_F/TM4_J		
RAT4_JM	TM4_M/TM4_J		
RAT4_FM	TM4_M/TM4_F		
DIFF2_JF	TM2_F − TM2_J		
DIFF2_JM	TM2_M − TM2_J		
DIFF2_FM	TM2_M − TM2_F		
RAT2_JF	TM2_F/TM2_J		
RAT2_JM	TM2_M/TM2_J		
RAT2_FM	TM2_M/TM2_F		

M, JF, JM, FM, and JFM) and summer image combinations (U, A, and UA) were used to calibrate models for estimating hardwood forest BA.

3.4. Predictive models

Partial least squares (PLS) regression is a strategy for constructing predictive models of response variables when predictors (factors) are numerous and highly collinear (Geladi & Kowalski, 1986; Wold et al., 2009). In cases where predictor variables are 1) relatively few, 2) not significantly redundant, and 3) have understood relationships to the response variable, multiple linear regression (MLR) is an acceptable modeling approach; otherwise MLR is inefficient or inappropriate (Tobias, 1995). PLS regression excels in the latter case by extracting relatively few latent predictors (X-scores) and latent responses (Y-scores), from respective X and Y data matrices, to indirectly predict the original set of response variables. In doing so, PLS regression mitigates unstable collinear effects in both X and Y data space (Helland, 1988), while the only assumption is that relationships between X and Y are linear (Wold et al., 2009). In addition, PLS regression does not assume zero error in the predictor data (often falsely assumed for image data, Curran & Hay, 1986). And, unlike principal components regression (PCR) where X-scores are extracted from an X-matrix of predictors (spectral decomposition of X′X) (Massy, 1965), PLS regression is more specific in that it involves singular decomposition of X′Y (i.e., predictor and response). Here, directions in latent variable space (associated with high variance in the response) are selected so that relationship strength between consecutive pairs of scores is maximized (Geladi & Kowalski, 1986; Tobias, 1995).

Because of these beneficial properties, PLS regression has been used to calibrate models of biochemical and biophysical forest parameters using full-spectrum (i.e. hyperspectral) imagery (Coops et al., 2003; Townsend et al., 2003; Martin et al., 2008; and many more). However, while PLS regression appropriately handles multicollinearity among predictors, it does not exclude weak predictor variables. Instead, unresponsive predictor variables (showing low or no responsiveness to the dependent variables) are simply deemphasized by assignment of near zero coefficient loadings. The result is that models remain unnecessarily large; especially in the case of hyperspectral (>200 bands) remote sensing applications.

To address this, PLS regression was recently used in an iterative processing stream with multi-temporal imagery to both simplify and strengthen forest parameter estimation models (Wolter et al., 2008). In this iterative process, each predictor variable is excluded from PLS model development then put back into the pool until all predictors have been excluded exactly once. The one excluded predictor variable which produced the best model (lowest RMSE of prediction) is then permanently discarded from the pool of predictor variables, whereby the iterative exclusion PLS (xPLS) process is repeated in this fashion until the RMSE of prediction can no longer be reduced—the final model. The xPLS method of model reduction is repeatable and has consistently produced more streamlined models with substantially higher precision of parameter estimation (Wolter & Townsend, 2011; Wolter et al., 2008, 2009).

In this study, we extend the use of xPLS to evaluate the 66 winter and 38 summer Landsat image predictor variables (Table 2) to calibrate models for estimating hardwood forest BA at SNWR. We compare both the merits of using winter versus summer Landsat data and single-date versus multi-date analyses. Leave-one-out cross-validation (Gong, 1986), using the prediction residual sum of squares (PRESS) procedure (Myers, 1986), was used to validate all models as there were limited observations, per the three BA classes described above, to permit splitting of the data into both development and validation datasets. This method of model validation is analogous to applying the equation to an independent dataset as the PRESS residual is obtained using observations that are excluded during equation derivation (Sun et al., 2003; Woods et al., 2008). Differences between regression slope parameters for all single- and multi-temporal BA model calibrations are evaluated using F-tests on squared residuals of the estimates.

4. Results

4.1. Single- and multi-date BA model calibration and cross-validation

Separate cross-validation of forest BA models calibrated using ground plot data and single-date, winter, Landsat imagery resulted in coefficients of determination (R^2) that ranged between 0.69 (PRESS = 0.526, RMSE = 3.67 $m^2 ha^{-1}$) and 0.81 (PRESS = 0.463, RMSE = 3.37 m^2 ha^{-1}) for 8 January 2008 (J) and 10 March 2008 (M), respectively (Table 3). Forest BA models calibrated using single-date summer imagery explained similar proportions of the variability in ground plot data (U, $R^2 = 0.71$ and A, $R^2 = 0.75$), but with generally higher PRESS and RMSE values on average (Table 3). Coincidence tests (H_o: agreement of slope parameters) between single-date BA model calibrations (winter J–F, F–M, and J–M; summer U–A; and winter to summer U–J, U–F, U–M, A–J, A–F, and A–M), show that F–M, U–A, U–J, and A–J regressions were not significantly different: $p = 0.280$, 0.665, 0.715, and 0.425, respectively (Table 4).

The three BA models calibrated using two-date combinations of winter Landsat data each had higher R^2 (JF, 0.78; JM, 0.86; and FM, 0.83), lower RMSE (3.68, 3.15, and 3.53 m^2 ha^{-1}, respectively), and lower PRESS values (0.490, 0.444, and 0.457, respectively) than the BA model calibrated using two dates of summer Landsat imagery: UA, $R^2 = 0.76$, RMSE = 3.85 m^2 ha^{-1}, and PRESS = 0.523 (Table 3). Coincidence tests (Table 4) indicated no significant differences between regression slope parameters of the three winter model calibrations (JF, JM, and FM), while the UA model's slope parameter was significantly different from all two-date winter models, especially JM and FM ($p = 0.000$ and 0.004, respectively). The JF and JM model slopes were marginally different ($p = 0.061$).

The one BA model calibrated using three dates of winter imagery (JFM) resulted in the highest R^2 (0.90), lowest RMSE (2.73 m^2 ha^{-1}),

Table 3
Results of xPLS regression model development and leave-one-out cross validation of BA estimates. Letter codes for image date combinations are in Table 1.

Image date Combination	RMSE (m^2 ha^{-1})	R^2	Adj. R^2	Root mean PRESS	Initial Vars.	No. Vars. Selected	No. of Factors	Regress. Intercept	Regress. Slope
JFM	2.729	0.898	0.897	0.403	66	13	11	1.945	0.898
JF	3.681	0.783	0.779	0.490	37	5	1	4.150	0.783
JM	3.146	0.861	0.859	0.444	37	13	10	2.660	0.861
FM	3.532	0.825	0.822	0.457	37	4	3	3.347	0.825
J	3.674	0.691	0.685	0.526	15	8	2	5.924	0.691
F	3.718	0.772	0.768	0.513	15	7	2	4.359	0.772
M	3.366	0.812	0.809	0.463	15	4	3	3.604	0.812
UA	3.845	0.762	0.758	0.523	15	12	4	4.551	0.762
U	4.080	0.714	0.709	0.529	15	8	2	5.467	0.714
A	3.919	0.749	0.744	0.524	36	8	4	4.815	0.749

Table 4
Comparisons between regression slope parameters for the ten forest BA models. Numbers represent two-tailed, F-test (1, 58) probabilities that variances in squared residuals ($[\hat{y}-y]^2$) among BA model calibrations are not significantly different. Significant slope differences ($p<0.05$) are in bold. Column/row headings represent date(s) of Landsat imagery used to calibrate respective BA models (letter date-codes are in Table 1).

	J	F	M	U	A	JF	JM	FM	UA
F	**0.0032**								
M	**0.0001**	0.2802							
U	0.7154	**0.0094**	**0.0003**						
A	0.4251	**0.0296**	**0.0013**	0.6647					
JF	**0.0001**	0.2745	0.9896	**0.0003**	**0.0012**				
JM	**0.0000**	**0.0033**	0.0596	**0.0000**	**0.0000**	**0.0613**			
FM	**0.0000**	0.0813	0.5036	**0.0000**	**0.0001**	0.5120	0.2218		
UA	0.0749	0.2316	**0.0236**	0.1555	0.3224	**0.0228**	**0.0000**	**0.0036**	
JFM	**0.0000**	**0.0000**	**0.0009**	**0.0000**	**0.0000**	**0.0010**	0.1417	**0.0076**	**0.0000**

lowest PRESS (0.403), intercept nearest to zero, and slope closest to unity for all models tested (Table 3). Regression slope differences between the JFM model and all other BA models, but the JM model ($p=0.142$), were highly significant (Table 4).

While the JFM BA model calibration was superior to all other models, the two-date JM model calibration closely rivaled JFM results (Table 3, Fig. 3), with a slope parameter that was substantially different from nearly all other BA models (Table 4). Among single-date BA models, the 10 March (M) 2008 (solar elevation 36.1°) calibration and cross-validation yielded R^2 (0.81), RMSE (3.37 m^2 ha^{-1}), and PRESS (0.463) values superior to 8 January (J) 2009 (solar elevation 18.5°), 23 February (F) 2008 (solar elevation 30.0°), and all summer (U, A, and UA) BA model calibrations combined (Table 3). While the March model's slope parameter was significantly different from all summer BA models, it was not different from either the JF or FM model and only marginally different from the JM model (Table 4).

4.2. Image predictor variables and BA model complexity

While the JFM and JM models were superior for predicting forest BA at SNWR, they were also more complex. In each case, xPLS regression retained 13 image predictor variables (five common to each model) with 11 and 10 latent factors used, respectively. In contrast, the next three strongest BA models (FM, M, and JF, respectively) retained four to five image predictor variables; each with one to three latent variables (Table 3, Fig. 4). The summer BA model calibration, UA, was also relatively complex; retaining 12 image variables (four latent factors). The summer single-date model calibrations, U and A, each retained eight image variables with two and four latent factors, respectively.

In the following results, positive and negative xPLS regression coefficient loading are indicated using '+' and '–' symbols, respectively, preceding the predictor variable name. For the JFM BA model, March shaded relief (+SHD_M) and January shortwave infrared to green normalized difference ratio (+ND25_J) had the top ranked coefficient loadings followed by January shaded relief (−SHD_J), March–January near-infrared (NIR) difference (−DIFF4_JM), and March-February NIR difference (−DIFF4_JM) (Fig. 4). The JM-based BA model, with a 17.6° difference in sun elevation angle between dates, was most strongly loaded on March–January NIR difference (−DIFF4_JM) followed closely by –SHD_J and +SHD_M. Both the JFM and JM models had moderate loading on the March–January ratio of green reflectance (+RAT2_JM). The JF-based BA model was the weakest of the multi-date, winter models, where NIR difference (−DIFF4_JF) had the strongest coefficient loading. Conversely, the FM-based BA model, with a 6.0° difference in solar elevation angle between dates, did not retain predictor variables consisting of date-wise band differences or ratios; nor were shaded relief variables retained. The xPLS calibration procedure for March (M) was the least complex of all BA models tested in that only four predictor variables (−M1, −ND42_M, −NDVI_M, and +ND32_M) were retained from one date of imagery. These four variables accounted for 81% of the variation (RMSE 3.37 m^2 ha^{-1}) in ground plot data, which is 9.6% and 5.7% less than the two best multi-date forest BA models: JFA (RMSE = 2.73 m^2 ha^{-1}) and JM (RMSE = 3.15 m^2 ha^{-1}), respectively (Table 3).

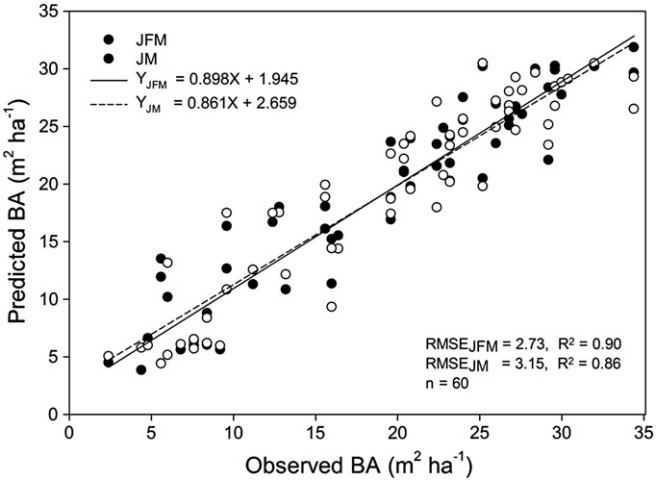

Fig. 3. Cross-validation results for hardwood BA model calibrations produced using xPLS regression with all three winter Landsat images (J, 1/8/2009; F, 2/23/2008; and M, 3/10/2008) and the best combination of two winter images (JM). While the JFM BA model calibration was superior to all single- and two-date image combinations, the JM BA model calibration rivaled JFM results (see Table 3).

5. Discussion

5.1. Sun angle, shadows, and multi-date analyses

The fact that the 10 March 2008 (M) BA model explained 81% (RMSE 3.37 m^2 ha^{-1}) of the variability in ground measurement data, with only four predictor variables incorporated into the xPLS, is remarkable (Table 3, Fig. 4). We suspect the better performance of the March BA model over the January (J) and February (F) models may be linked to higher sun elevation angle (36.1° vs. 30.0 and 18.5). Even though the three winter BA xPLS models made use of different numbers of predictors, there does appear to be some empirical evidence of a relationship between BA model performance (measured by R^2) and solar elevation angle at the time of sensor overpass. Whether or not this relates to tree shadow size, degree of canopy self-shading, terrain shading effects (see Vikhamar & Solberg, 2002), or some combination of all of these factors remains unresolved. We doubt that snow retention on tree branches was a contributing factor due to wind force after recent snow fall events prior to each winter image acquisition (Table 1).

While the two single-date, summer, BA models produced good results, explaining 71% (U) and 75% (A) of the variability in ground plot

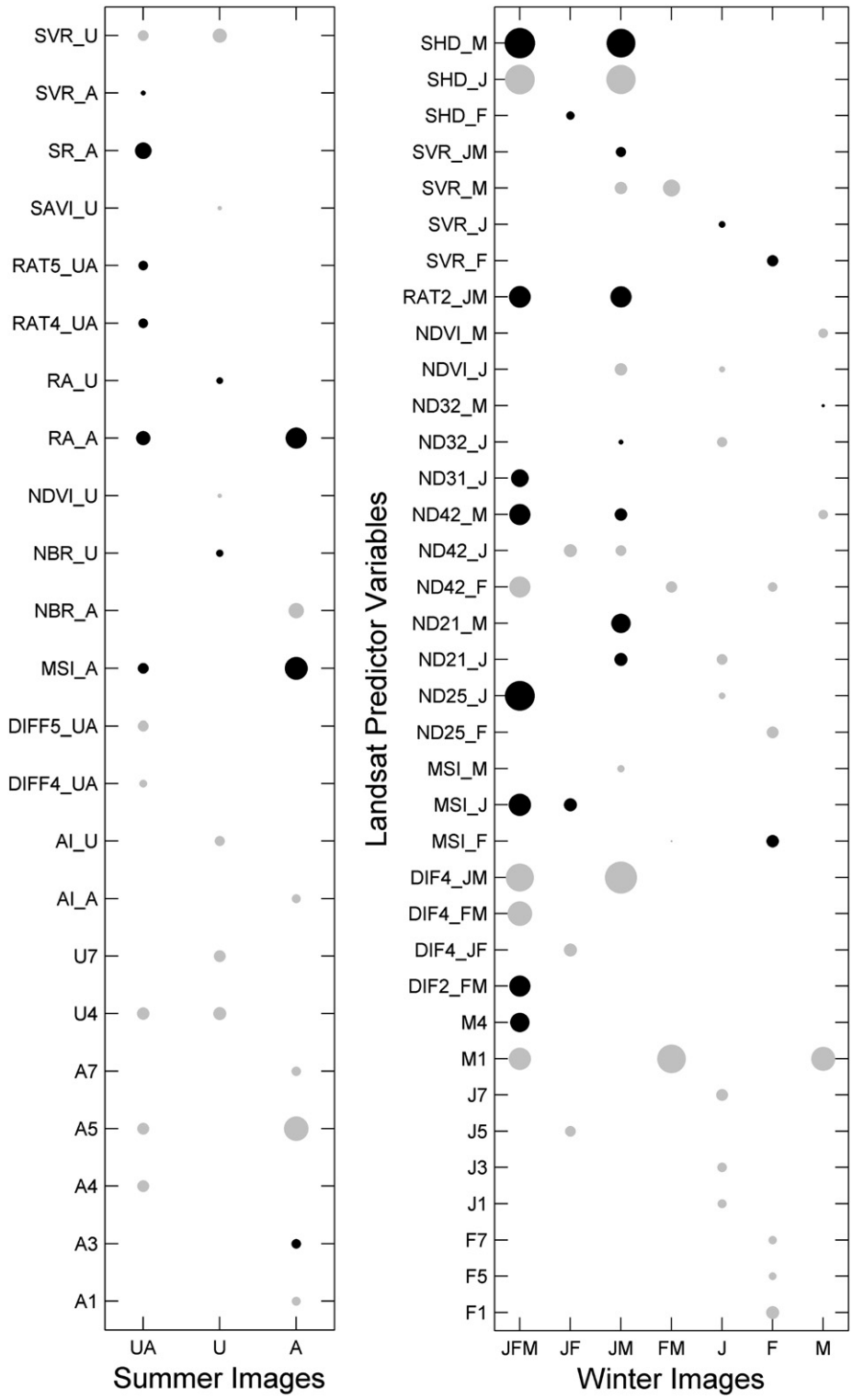

Fig. 4. Scaled component loadings for xPLS-selected image predictor variables by date combination (J, 1/8/2009; F, 2/23/2008; M, 3/10/2008; U, 6/30/2008; and A, 8/17/2008). The ordinates of the winter (left) and summer (right) graphs list all image variables used by at least one of the forest BA models from the total variable sets tested (Table 2). Positive and negative loadings are depicted as black and gray filled circles, respectively, while circle size indicates loading magnitude. The two best BA models (JFM and JM, Table 3, Fig. 3) each used 13 image predictor variables accounting for 80.3% (JFM, 1–13/66) and 65.8% (JM, 1–13/38) model reductions, respectively. These two BA models were each strongly loaded on shaded relief (SHD_J and SHD_M) and on Landsat variables formulated specifically to enhance tree shadow differences: date-wise reflectance differences in the near-infrared (DIFF4_MJ) and date-wise ratio of green reflectance (RAT2_MJ).

data (Table 3), we conclude that, in terms of both model simplicity and accuracy, single-date, winter, Landsat imagery, with snow ground cover, are better suited for estimating hardwood forest BA at SNWR. Whether it is worth the effort to add one or two more winter images (having different solar ephemeris) to explain an additional 10% of the variance in measured BA is subjective. These results parallel those of Wolter et al. (2008) who concluded that the greater relative strength of predictive variables derived from winter Landsat data in estimating forest BA in northern Minnesota were likely the result of advantages (over imagery from other seasons) that snow

ground cover provides. In addition to the merits of tree shadow and snow illumination differences, we also note that atmospheric moisture is typically much lower during winter months in this region compared to summer. This may improve Landsat band signal to noise ratios and, hence, bolster winter-based BA model performance, although the tradeoff of increased atmospheric clarity is likely balanced by reduced SNR due to lower solar energy.

We were puzzled by the relative importance of visible blue (TM1) for the March BA model considering that TM1 was excluded from both January and February model calibrations. We speculate that as sun elevation increases, radiometric saturation in TM1 is more pronounced over snow cover (e.g., Dozier, 1989) causing possible loss of fine-branch sun-lit/shadow contrast (including understory brush). In this scenario, Landsat's blue sensor may be relatively blind to smaller ground-shadows and/or canopy signatures and more strongly biased toward signatures produced by the larger forest components (boles and large branches). Whether this is the case is the subject for future investigation.

When multiple dates of winter Landsat imagery were used, date-wise difference variables were among the strongest predictors of forest BA at SNWR (Fig. 4). For instance, for the JM (January–March) model, where the temporal change in sun elevation angle between dates was greatest (17.55°, see Table 1), it was not surprising that difference variables provided the strongest predictors of hardwood forest BA. For example, assuming an average tree height of 16.76 m at SNWR, a 17.55° difference (Δ) in sun elevation angle between image dates (8 Jan.–10 Mar.) translates to potential changes in tree ground-shadow length of as much as 25.7 m; compared to 21.1 m and 4.6 m shadow differences for J–F (Δ 11.54°) and F–M (Δ 6.01°) time periods, respectively. As far as the authors are aware, exactly how sun angle differences affect spatially integrated proportion of shaded forest floor visible to satellite sensors, such as Landsat, under leafless forest conditions and varying BA has not been investigated. For JFM, JM, and JF, the observation that NIR change variables (e.g., DIFF4_MJ and DIFF4_MF) had stronger coefficient loadings than visible green and short wave infrared (SWIR) change variables (Fig. 4) may be due to stronger overall contrast sensitivity between hard, geometric shadow and illuminated snow. Factors that may contribute to the observed importance of NIR change variables include relative signal to noise ratios (negligible Rayleigh scattering), lower sensitivity of the NIR than visible green to atmospheric moisture conditions (Green, 2001), lower sensitivity to snow moisture status compared to SWIR, and less sensitivity to snow grain size compared to longer NIR wavelengths (Painter et al., 2003).

The inclusion of the January ND25 (+ND25_J) predictor (also known as the normalized difference snow index, NDSI, Dozier, 1989) in the JFM forest BA model (and the J model) was not as surprising as was the relative strength (second strongest) of this variable (Fig. 4, Table 2). While snow depth varied by date (max. difference = 15 cm), such differences were assumed to be inconsequential to these analyses so long as the forest floor remained completely covered (see Vikhamar & Solberg, 2002) and understory was not dominated by brush, which is the case at SNWR (Fig. 1B). Nevertheless, because the January image was 1) collected under the lowest sun elevation angle (18.5°), 2) the coldest temperature (−18.9°°C), and 3) had the deepest (42.5 cm) snow cover (Table 1), it begs the question whether snow properties (grain size, liquid water, or chemical impurities: dust, soot, pollen), other than depth, were unique on this date since NDSI is known to be somewhat sensitive to snow-surface attributes (Dozier, 1989). Nevertheless, our ground data and modeling results provide no specific conclusions regarding such effects or the strong loading of the ND25 variable compared to similar variables (e.g., SVR), beyond the general wavelength-dependent illumination/shadow contrast differences we already discussed.

Considering the performance of the JFM and JM forest BA models (Tables 3, 4), it seems reasonable to suggest that differences in reflectance detected by Landsat between winter months provide strong complementary predictive information for estimating forest BA beyond what is possible using single-date analyses alone. Contributing factors include 1) optimal spectral contrast on bright snow ground cover, 2) sun elevation-driven shadow characteristics, and 3) forest floor illumination/shadow proportion.

For summer, the four multi-temporal change variables −DIFF5_UA, +RAT4_UA, +RAT5_UA, and −DIFF4_UA (in order of loading magnitude) retained during xPLS calibration of the June–August (UA) model were not among the top five strongest predictors of BA (Fig. 4). These variables were originally included to be consistent with the analyses of winter images. Temporal changes in canopy shading, due to sun elevation (8.9°) and azimuth (8.2°), or lags in oak canopy foliar development (see Wolter et al., 1995) probably contributed to the retention of these June–August image change variables. However, the within-canopy dynamics of shadows among leaf-on forest canopies are more closely related to leaf area index (LAI), crown shape, and tree density (Kucharik et al., 1998; Song & Woodcock, 2002) than to shadows cast onto the forest floor, as with the winter difference images. During leaf-off periods, temporal change variables are sensitive to branch area index (BAI) and the shadows cast onto the ground. This points to important differences in the behavior of shadows in multi-temporal imagery. For example, summer crown projection may vary less with sun elevation due to its ellipsoidal shape compared to a collection of branches (cylinders) in a crown with related shadows cast. As such, differences in proportions of sun-lit and shaded forest elements (especially forest floor) through the winter months are the only reasonable explanation for the observed predictive strength of Landsat, change variables (i.e., DIFF4_JM, DIFF4_FM, and RAT2_JM) for estimating forest BA at SNWR (Fig. 4). Hence, our results indicate a stronger allometric link between BAI-driven shadows to BA than canopy-driven reflectance links observed under leaf-on summer conditions (e.g., Wolter et al., 2008). Franco-Lopez et al. (2001) came to a similar conclusion that information gleaned from winter Landsat imagery appeared to be associated more to forest volume and BA (functions of tree occupancy of a pixel) than to specific vegetation radiance, as in summer months.

Differences in terrain shading between 8 January (SHD_J) and 10 March (SHD_M) also explained variations between measured BA and forest spectral responses among both the January–March (JM) and January–February–March (JFM) models (Fig. 4). Given the 17.55° change in sun elevation angle between these dates, it is reasonable to suggest that these shaded-relief variables help to resolve differences in tree shadow-fraction that vary as functions both BA and shadow distortion due to local terrain. Hence, inclusion of both SHD_J and SHD_M in the calibration of the JM and JFM models may serve as correction factors for such differences, with stronger impacts as predictors when differences in sun elevation are greater. In fact, we suspect that higher overall sun elevation angles later in the winter (fewer terrain effects), and the slight relative difference between 23 February and 10 March (6.01°), explain why the associated shaded relief variables (SHD_F and SHD_M) were not retained during calibration of the February–March (FM) model (Fig. 4), but were retained for both JM and JFM model calibrations. It should be reiterated that topographic corrections performed on imagery prior to analyses simply adjusts for reduced reflectance of incident solar irradiance due to sun orientation with respect to local terrain; not effects on tree shadow length or relative contrast.

5.2. Future work

Use of winter Landsat sensor data to estimate forest BA is not entirely novel (Franco-Lopez et al., 2001; Wolter & Townsend, 2011; Wolter et al., 2008). However, use of multi-temporal winter imagery (with snow cover) to explore empirical relationships between deciduous forest basal area and Landsat's spatially integrated view of leaf-off forest, shadows cast on the ground, and ground shadow/illumination differences with changes in solar geometry has not been reported. While the empirical results of this study are encouraging, specific conclusions

are premature regarding the drivers between forest BA and Landsat-detected tree shadows or temporal changes in forest floor shadow-fraction (driven by sun elevation angle differences). Spectral end member analysis or other modeling techniques, such as geometric–optical models adapted to account for leaf-off properties (e.g., LeBlanc et al., 1999), could be used to specifically characterize angular distribution patterns of reflected solar irradiance from leaf-off deciduous forests.

The forest basal area models developed for the SNWR are not refuge-specific, but they may be specific to general forest functional types such as hardwood, conifer, and mixed wood. This is because winter shading patterns across these general forest types will vary according to tree architecture (Chen & Leblanc, 1997; Greenberg et al., 2005; Li & Strahler, 1985), thus affecting any potential relationships to forest BA. As a result, it is necessary to test how robust this approach may be for other hardwood forest types (e.g., *Populus* sp., *Betula* sp., and *Acer* sp.), conifer types, and mixtures of each. Successful characterization of these relationships will pave the way for broader landscape analyses including scaling up to regional extents using sensors such the Indian Space Agency's Advanced Wide Field Sensor (AWiFS, 740 km swath) and NASA's Moderate Resolution Imaging Spectroradiometer (MODIS, 2330 km swath).

6. Conclusions

From these analyses we conclude that winter Landsat imagery with complete snow cover on the ground and high sun elevation angle, are better suited to calibrating hardwood forest BA models than either single- or multi-date summer Landsat imagery. Winter imagery provides a unique view of the forest floor that is spectrally simple (consisting predominantly of sunlit and shaded tree bark and snow) compared to snowless, leaf-off conditions in either spring or autumn. Maximum spectral contrast, afforded by snow cover, enables optimal detectability of these basic signatures and facilitates leveraging of suspected geometric/allometric links with forest biophysical parameters. We theorize that winter-specific detectability of tree shadow geometries is the key to greater accuracy and simplicity in calibrating our empirical oak forest BA models at SNWR: imagery from 10 March 2008 (sun elevation angle 36.1°) produced the best single-date model. Further improvements in model calibration were achieved by combining two and three winter Landsat images having substantially different solar elevation ephemeris (e.g., 8 January 2009, Δ 17.6°). Among the latter analyses, date-wise differences in NIR reflectance and shaded relief were especially important. Under winter conditions with snow-covered ground, it is reasonable to presume that tree shadows cast on the forest floor and differences in shadow geometries, due to changes in sun elevation angle, produce unique forest reflectance signatures.

We agree with Vikhamar and Solberg (2002) that structural correlations between canopy shadows and actual forest attributes such as BA or biomass are unlikely to be 1:1 under continuous forest cover conditions, due to inter-canopy self-shading. However, our analyses have shown that the combination of two or more dates of winter Landsat imagery improved estimation of forest BA over common approaches using either single-date analyses or multi-temporal summer image analyses. The degree to which canopy self-shading may have affected these multi-date winter image analyses is not known. However, answers to these questions may also be investigated in the future through use of canopy reflectance modeling techniques (Chen & Leblanc, 1997; Leblanc et al., 1999; Li & Strahler, 1985). Hence, the key to extending these methods for regional analyses rests in understanding the relationships between forest shading patterns and BA across general forest functional types.

Acknowledgments

This research was supported by funding from the U.S. Fish and Wildlife Service, as well as fellowship support from the Department of Forest and Wildlife Ecology at the University of Wisconsin. We would also like to thank the three anonymous reviewers for constructive comments that greatly improved the quality of this manuscript.

References

Anderson, J. E., Plourde, L. C., Martin, M. E., Braswell, B. H., Smith, M. -L., Dubayah, R. O., et al. (2008). Integrating waveform lidar with hyperspectral imagery for inventory of a northern temperate forest. *Remote Sensing of Environment*, *112*, 1856–1870.

Arzani, H., & King, G. W. (1997). Application of remote sensing (Landsat TM data) for vegetation parameters measurement in western division of NSW. *Proceedings XVIII IGC 1997 Winnepeg, Manitoba*.

Badhwar, G. D., MacDonald, R. B., Hall, F. G., & Carnes, J. G. (1985). Spectral characterization of biophysical characteristics in the boreal forest: relationship between TM band reflectance and LAI for aspen. *IEEE Transactions on Geoscience and Remote Sensing*, *GE-24*, 322–326.

Blais, J. R. (1958). The vulnerability of balsam fir to spruce budworm attack in northwestern Ontario, with special reference to the physiological age of the tree. *Forestry Chronicle*, *34*(4), 405–422.

Brockhaus, J. A., Khorram, S., Bruck, R. I., Campbell, M. V., & Stallings, C. (1992). A comparison of Landsat TM and SPOT HRV data for use in the development of forest defoliation models. *International Journal of Remote Sensing*, *13*(16), 3235–3240.

Brown, L., Chen, J. M., Leblanc, S. G., & Cihlar, J. (2000). A shortwave infrared modification to the simple ratio for LAI retrieval in boreal forests: An image and model analysis. *Remote Sensing of Environment*, *71*, 16–25.

Brown, S., Gillespie, A. J. R., & Lugo, A. E. (1989). Biomass estimation methods for tropical forests with applications to forest inventory data. *Forest Science*, *35*(4), 881–902.

Buchanan, H. (1996). Oak savanna restoration at Myre-Big Island State Park. Internet source:. http://horticulture.cfans.umn.edu/vd/h5015/96papers/buchanan.htm

Burrows, S. N., Gower, S. T., Norman, J. M., Diak, G., Mackay, D. S., Ahl, D. E., et al. (2003). Spatial variability of aboveground net primary production for a forested landscape in northern Wisconsin. *Canadian Journal of Forest Research*, *33*, 2007–2018.

Chen, J. M., & Cihlar, J. (1996). Retrieving leaf area index of boreal conifer forests using Landsat TM images. *Remote Sensing of Environment*, *55*, 153–162.

Chen, J. M., & Leblanc, S. G. (1997). A four-scale bidirectional reflectance model based on canopy architecture. *IEEE Transactions on Geoscience and Remote Sensing*, *35*(5), 1316–1337.

Cohen, W. B., & Spies, T. A. (1992). Estimating structural attributes of douglas–fir/western hemlock forest stands from Landsat and SPOT imagery. *Remote Sensing of Environment*, *41*, 1–17.

Coops, N. C., Smith, M. L., Martin, M. E., & Ollinger, S. V. (2003). Prediction of eucalypt foliage nitrogen content from satellite-derived hyperspectral data. *IEEE Transactions on Geoscience and Remote Sensing*, *41*(6), 1338–1346.

Culvenor, D. S., & Coops, N. C. (1999). A forest scene simulation model based on geometric optics. *Abstracts of the Second International Workshop on Multiple-Angle Measurements and Models, Ispra, Italy, September 15–17*.

Curran, P., & Hay, A. (1986). The importance of measurement error for certain procedures in remote sensing at optical wavelengths. *Photogrammetric Engineering and Remote Sensing*, *52*(2), 229–241.

Dozier, J. (1989). Spectral signature of alpine snow cover from the landsat thematic mapper. *Remote Sensing of Environment*, *28*, 9–22.

Dubayah, R. C. (1994). Modeling a solar radiation topoclimatology for the Rio Grande River Basin. *Journal of Vegetation Science*, *5*, 627–640.

Franco-Lopez, H., Ek, A. R., & Bauer, M. E. (2001). Estimation and mapping of forest stand density, volume, and cover type using the k-nearest neighbors method. *Remote Sensing of Environment*, *77*, 251–274.

Franklin, J. (1986). Thematic Mapper analysis of coniferous forest structure and composition. *International Journal of Remote Sensing*, *7*(10), 1287–1301.

Franklin, J., & Strahler, A. H. (1988). Invertible canopy reflectance modeling of vegetation structure in semiarid woodland. *IEEE Transactions on Geoscience and Remote Sensing*, *26*, 809–825.

Geladi, P., & Kowalski, B. R. (1986). Partial least-squares regression: A tutorial. *Analytica Chimica Acta*, *185*, 1–17.

Ginrich, S. F. (1967). Measuring and evaluating stocking and stand density in upland hardwood forests in the central States. *Forest Science*, *13*(1), 38–53.

Gong, G. (1986). Cross-validation, the jackknife, and the bootstrap: Excess error estimation in forward logistic regression. *Journal of the American Statistical Association*, *81*(393), 108–113.

Green, R. O. (2001). Atmospheric water vapor sensitivity and compensation requirement for Earth-looking imaging spectrometers in the solar-reflected spectrum. *Journal of Geophysical Research*, *106*(D15), 17443–17452.

Greenberg, J. A., Dobrowski, S. Z., & Ustin, S. L. (2005). Shadow allometry: Estimating tree structural parameters using hyperspatial image analysis. *Remote Sensing of Environment*, *97*, 15–25.

Grosenbaugh, L. R. (1952). Plotless timber estimates-New, fast, easy. *Journal of Forestry*, *50*, 322–337.

Gupta, R. P., Haritashya, U. K., & Singh, P. (2005). Mapping dry/wet snow cover in the Indian Himalayas using IRS multispectral imagery. *Remote Sensing of Environment*, *97*, 458–469.

Helland, I. S. (1988). On the structure of partial least squares regression. *Communications in Statistics—Simulation and Computation*, *17*(2), 581–607.

Horler, D. N. H., & Ahern, F. J. (1986). Forestry information content of thematic mapper data. *International Journal of Remote Sensing*, *7*, 405–428.

Hudak, A. T., Crookston, N. L., Evans, J. S., Falkowski, M. J., Smith, A. M. S., Gessler, P. E., et al. (2006). Regression modeling and mapping of coniferous forest basal area and tree density from discrete-return lidar and multispectral satellite data. *Canadian Journal of Remote Sensing*, *32*(2), 126–138.

Huete, A. R. (1988). A soil adjusted vegetation index (SAVI). *Remote sensing of the environment*, *25*, 295–309.

Hyyppä, J., Hyyppä, H., Inkinen, M., Engdahl, M., Linko, S., & Zhu, Y. -H. (2000). Accuracy comparison of various remote sensing data sources in the retrieval of forest stand attributes. *Forest Ecology and Management*, *128*, 109–120.

Jenkins, J. C., Chojnacky, D. C., Heath, L. S., & Birdsey, R. A. (2003). National-scale biomass estimators for United States tree species. *Forest Science*, *49*(1), 12–35.

Jordan, C. F. (1969). Derivation of leaf area index from quality of light on the forest floor. *Ecology*, *50*, 663–666.

Jordan, R. (1991). A one-dimensional temperature model for a snow cover: technical documentation for NSTHERM.89', Spec. Rep. 91-16. *US Army Corps of Eng., Cold Reg. Res. and Eng. Lab., Hanover, New Hampshire*.

Key, C. H., & Benson, N. C. (2005). Landscape assessment: Remote sensing of severity, the Normalized Burn Ratio. In D. C. Lutes (Ed.), *FIREMON: Fire effects monitoring and inventory system. General Technical Report, RMRSGTR-164-CD: LA1–LA51*. Ogden, UT: USDA Forest Service, Rocky Mountain Research Station.

Kucharik, C. J., Norman, J. M., & Gower, S. T. (1998). Measurements of branch area and adjusting leaf area index indirect measurements. *Agricultural and Forest Meteorology*, *91*, 69–88.

Larsen, N. F., & Stamnes, K. (2005). Use of shadows to retrieve water vapor in hazy atmospheres. *Applied Optics*, *44*(32), 6986–6994.

Law, J. R., Johnson, P. S., & Houf, G. (1994). A crown cover chart for oak savannas. Silviculture and Ecology Upland Central Hardwood Forests Research Unit. U.S. Department of Agriculture, Forest Service. (Internet source:). http://ncrs.fs.fed.us/pubs/tb/tb2/techbrf2.html

LeBlanc, S. G., Bicheron, P., Chen, J. M., Leroy, M., & Cihlar, J. (1999). Investigation of directional reflectance in boreal forests with an improved four-scale model and airborne POLDER data. *IEEE Transactions on Geoscience and Remote Sensing*, *37*(3), 1396–1414.

Leboeuf, A., Beaudoin, A., Fournier, R. A., Guindon, L., Luther, J. E., & Lambert, M. -C. (2007). A shadow fraction method for mapping biomass of northern boreal black spruce forests using QuickBird imagery. *Remote Sensing of Environment*, *110*, 488–500.

Li, X., & Strahler, A. H. (1985). Geometric–optical modeling of a conifer forest canopy. *IEEE Transactions on Geoscience and Remote Sensing*, *GE-23*(5), 705–721.

Li, X., & Strahler, A. H. (1992). Geometric-optical bidirectional reflectance modeling of the discrete-crown vegetation canopy: Effect of crown shape and mutual shadowing. *IEEE Transactions on Geoscience and Remote Sensing*, *30*, 276–292.

Liang, S., Fang, H., Morisette, J. T., Chen, M., Shuey, C. J., Walthall, C. L., et al. (2002). Atmospheric correction of Landsat ETM + land surface imagery—Part II: Validation and applications. *IEEE Transactions on Geoscience and Remote Sensing*, *40*(12), 2736–2746.

Lim, K., Treitz, P., Baldwin, K., Morrison, I., & Green, J. (2003). Lidar remote sensing of biophysical properties of tolerant hardwood forests. *Canadian Journal of Remote Sensing*, *29*(5), 658–678.

Lopez-Garcia, M. J., & Caselles, V. (1991). Mapping burns and natural reforestation using Thematic Mapper data. *Geocarto International*, *1*, 31–37.

Marshall, J. D., & Waring, R. H. (1986). Comparison of methods of estimating leaf-area index in old-growth Douglas-fir. *Ecology*, *67*(4), 975–979.

Martin, M. E., Plourde, L. C., Ollinger, S. V., Smith, M. -L., & McNeil, B. E. (2008). A generalizable method for remote sensing of canopy nitrogen across a wide range of forest ecosystems. *Remote Sensing of Environment*, *112*, 3511–3519.

Massy, W. F. (1965). Principal components regression in exploratory statistical research. *Journal of the American Statistical Association*, *60*(309), 234–256.

McRoberts, R. E. (2008). A two-step nearest neighbors algorithm using satellite imagery for predicting forest structure within species composition classes. *Remote Sensing of Environment*, *113*, 532–545.

McRoberts, R. E., Tomppo, E. O., Finley, A. O., & Heikkinen, J. (2007). Estimating areal means and variances of forest attributes using the k-Nearest Neighbors technique and satellite imagery. *Remote Sensing of Environment*, *111*, 466–480.

Minnesota Department of Natural Resources (2005). *Field guide to the native plant communities of Minnesota: The Eastern Broadleaf Forest Province. Ecological Land Classification Program, Minnesota county Biological Survey, and Natural Heritage and Nongame Research Program. MNDNR St. Paul, MN, USA.*

Moisen, G. G., Freeman, E. A., Blackard, J. A., Frescino, T. S., Zimmermann, N. E., & Edwards, T. C. (2006). Predicting tree species presence and basal area in Utah: A comparison of stochastic gradient boosting, generalized additive models, and tree-based methods. *Ecological Modelling*, *199*, 176–187.

Myers, R. H. (1986). *Classical and modern regression with applications.* Boston: PWS-Kent publishing.

Niemi, G. J., & Hanowski, J. M. (1984). Relationships of breeding birds to habitat characteristics in logged areas. *Journal of Wildlife Management*, *48*(2), 438–443.

Oladi, D. (2001). Developing forest growth monitoring model using thematic mappery imagery. *Proceedings of the 22th Asian conference on remote sensing, 5–9 November, Singapore, Indonesia*.

Olsson, H. (1994). Changes in satellite-measured reflectances caused by thinning cuttings in boreal forest. *Remote Sensing of Environment*, *50*, 221–230.

Olyphant, G. A. (1984). Insolation topoclimates and potential ablation in alpine snow accumulation basins: Front Range, Colorado. *Water Resources Research*, *20*(4), 491–498.

Ozdemir, I. (2008). Estimating stem volume by tree crown area and tree shadow area extracted from pan-sharpened Quickbird imagery in open Crimean juniper forests. *International Journal of Remote Sensing*, *29*(19), 5643–5655.

Pacala, S. W., & Deutschman, D. H. (1995). Details that matter: The spatial distribution of individual trees maintains forest ecosystem function. *Oikos*, *74*, 357–365.

Painter, T. H., Dozier, J., Roberts, D. A., Davis, R. E., & Green, R. O. (2003). Retrieval of subpixel snow-covered area and grain size from imaging spectrometer data. *Remote Sensing of Environment*, *85*, 64–77.

Pastor, J., Dewey, B., Moen, R., Mladenoff, D. J., White, M., & Cohen, Y. (1998). Spatial patterns in the moose–forest–soil ecosystem on Isle Royale, Michigan, USA. *Ecological Applications*, *8*(2), 411–424.

Peddle, D. R., Hall, F. H., & LeDrew, E. F. (1999). Spectral mixture analysis and geometric–optical reflectance modeling of boreal forest biophysical structure. *Remote Sensing of Environment*, *67*, 288–297.

Perala, D. A., & Alban, D. H. (1994). Allometric biomass estimators for aspen-dominated ecosystems in the Upper Great Lakes. *U.S. Forest Service Research Paper NC-134* (pp. 38).

Phillips, O. L., Malhi, Y., Higuchi, N., Laurance, W. F., Núñez, P. V., Vásquez, R. M., et al. (1998). Changes in the carbon balance of tropical forests: Evidence from long-term plots. *Science*, *282*, 439–442.

Riaño, D., Chuvieco, E., Salas, J., & Aguado, I. (2003). Assessment of different topographic corrections in Landsat-TM data for mapping vegetation types. *IEEE Transactions on Geoscience and Remote Sensing*, *41*(5), 1056–1061.

Rock, B. N., Vogelmann, J. E., Williams, D. L., Vogelmann, A. F., & Hoshizaki, T. (1986). Remote detection of forest damage. *Bioscience*, *36*(7), 439–445.

Rogers, E. J. (1949). Estimating tree heights from shadows on vertical aerial photographs. *Journal of Forestry*, *47*(3), 182–191.

Rosenthal, W., & Dozier, J. (1996). Automated mapping of montane snow cover at subpixel resolution from the Landsat Thematic Mapper. *Water Resources Research*, *32*(1), 115–130.

Rouse, J. W., Haas Jr., R. H., Schell, J. A., & Deering, D. W. (1974). Monitoring vegetation systems in the Great Plains with ERTS. *Third ERTS Symposium, NASA SP-351*, *1*, 309–317.

Sayn-Wittgenstein, L. (1961). Phenological aids to tree species identification on air photographs. *Technical Note No. 104, Forest Research Branch, Canada Department of Forestry, Ottawa* (26 pp.).

Seeley, H. E. (1942). Tree heights from shadows. *Photogrammetric Engineering*, *8*, 100–109.

Seely, H. E. (1949). Air photography and its application to forestry. *Photogrammetric Engineering*, *15*(4), 548–554.

Sharov, A. A., Pijanowski, B. C., Liebhold, A. M., & Gage, S. H. (1999). What affects the rate of gypsy moth (Lepidoptera: Lymantriidae) spread: Winter temperature or forest susceptibility? *Agriculture and Forest Entomology*, *1*, 37–45.

Song, C. (2007). Estimating tree crown size with spatial information of high resolution optical remotely sensed imagery. *International Journal of Remote Sensing*, *28*(15), 3305–3322.

Song, C., & Woodcock, C. E. (2002). The spatial manifestation of forest succession in optical imagery. *Remote Sensing of Environment*, *82*, 271–284.

Song, C., & Woodcock, C. E. (2003). Estimating tree crown size from multiresolution remotely sensed imagery. *Photogrammetric Engineering and Remote Sensing*, *69*(11), 1263–1270.

Strahler, A. H., Wu, Y., & Franklin, J. (1988). Remote estimation of tree size and density from satellite imagery by inversion of a geometric-optical canopy model. *Proceedings: 22nd International Symposium on Remote Sensing of Environment, Abidjan,Ivory Coast, 20-26 October, Ann Arbor, MI* (pp.377–348).

Suits, G. H. (1972). The calculation of the directional reflectance of a vegetative canopy. *Remote Sensing of Environment*, *2*, 117–125.

Sun, S. J., Chumlea, W. C., Heymsfield, S. B., Lukaski, H. C., Schoeller, D., Friedl, K., et al. (2003). Development of bioelectrical impedance analysis prediction equations for body composition with the use of a multicomponent model for use in epidemiologic surveys. *American Journal of Clinical Nutrition*, *77*, 331–340.

Swain, P.C. (1972). An analysis of the morphological differences among oaks in selected stands of the *Quercus borealis–Q. ellipsoidalis* complex. M.S. Thesis, University of Minnesota, Minneapolis, MN, USA.

Tester, J. R. (1989). Effects of fire frequency on oak savannah in east-central Minnesota. *Bulletin of the Torrey Botanical Club*, *121*(3), 266–276.

Thome, K. J., Helder, D. L., Aaron, D., & Dewald, J. D. (2004). Landsat-5 TM and Landsat-7 ETM+ absolute radiometric calibration using the reflectance-based method. *IEEE Transactions on Geoscience and Remote Sensing*, *42*(12), 2777–2785.

Tobias, R. D. (1995). An introduction to partial lest squares regression. *Proceedings of the 20th Annual SAS User Group International (SUGI) conference, 2–5 April, Orlando, FL* (8pp.).

Townsend, P. A., Foster, J. R., Chastain, R. A., & Currie, W. S. (2003). Application of imaging spectroscopy to mapping canopy nitrogen in the forests of the central appalachian mountains using Hyperion and AVIRIS. *IEEE Transactions on Geoscience and Remote Sensing*, *41*(6), 1347–1354.

Van Brummelen, G., & Butler, B. (1997). Determining the interdependence of historical astronomical tables. *Journal of the American Statistical Association*, *92*(437), 41–48.

Verhoef, W. (1984). Light scattering by leaf layers with application to canopy reflectance modeling: The SAIL model. *Remote Sensing of Environment*, *16*(2), 125–141.

Vikhamar, D., & Solberg, R. (2002). Subpixel mapping of snow cover in forests by optical remote sensing. *Remote Sensing of Environment*, *84*, 69–82.

Vikhamar, D., Solberg, R., & Seidel, K. (2004). Reflectance modeling of snow-covered forests in hilly terrain. *Photogrammetric Engineering and Remote Sensing*, *79*(9), 1069–1079.

White, H. P., Miller, J. P., Chen, J. M., & Peddle, D. R. (1995). Seasonal change in mean understory reflectance for boreal sites: preliminary results. *Proceedings of the 17th Canadian Symposium on Remote Sensing (pp. 189–194), 13–15 June, Saskatoon, Saskatchewan, Canada.*

Whittaker, R. H., Bormann, F. H., Likens, G. E., & Siccama, T. G. (1974). The Hubbard Brook Ecosystem Study: Forest biomass and production. *Ecological Monographs*, *44*, 233–254.

Wold, S., Hoy, M., Martens, H., Trygg, J., Westad, F., MacGregor, J., et al. (2009). The PLS model space revisited. *Journal of Chemometrics*, *23*(2), 67–68.

Wolter, P. T., Mladenoff, D. J., Host, G. E., & Crow, T. R. (1995). Improved forest classification in the northern Lake State using multi-temporal Landsat imagery. *Photogrammetric Engineering and Remote Sensing*, *61*(9), 1129–1143.

Wolter, P. T., & Townsend, P. A. (2011). Estimating forest species composition using a multi-sensor fusion approach. *Remote Sensing of Environment*, *115*, 671–691.

Wolter, P. T., Townsend, P. A., Kingdon, C. C., & Sturtevant, B. R. (2008). Remote sensing of the distribution and abundance of host species for spruce budworm in northern Minnesota and Ontario. *Remote Sensing of Environment*, *112*, 3971–3982.

Wolter, P. T., Townsend, P. A., & Sturtevant, B. R. (2009). Estimation of forest structural parameters using 5 and 10 meter SPOT-5 satellite data. *Remote Sensing of Environment*, *113*, 2019–2036.

Woods, M., Lim, K., & Treitz, P. (2008). Predicting forest stand variables from LiDAR data in the Great Lakes–St. Lawrence forest of Ontario. *The Forestry Chronicle*, *84*(6), 827–839.

Wovcha, D. S., Delaney, B. C., & Nordquist, G. E. (1995). *Minnesota's St. Croix River Valley and Anoka Sandplain: A guide to native habitats.* Minneapolis: University of Minnesota Press.

Wu, Y., & Strahler, A. H. (1994). Remote estimation of crown size, stand density, and biomass on the Oregon transect. *Ecological Applications*, *4*(2), 299–312.

Wulder, M., Niemann, K. O., & Goodenough, D. G. (2000). Local maximum filtering for the extraction of tree locations and basal area from high spatial resolution imagery. *Remote Sensing of Environment*, *73*, 103–114.

Zheng, D., Heath, L. S., & Ducey, M. J. (2008). Satellite detection of land-use change and effects on regional forest aboveground biomass estimates. *Environmental Monitoring and Assessment*, *144*, 67–70.